Research Article GU J Sci, Part A, 10(1): 53-61 (2023) 10.54287/gujsa.1202745

Gazi University
Journal of Science
PART A: ENGINEERING AND INNOVATION
http://dergipark.org.tr/gujsa

A Study on the Wide Frequency Range Electrical Variables in the Al/Coumarin–PVA/p-Si Diodes at Room Temperature

Selçuk DEMİREZEN[1*]

[1]*Sabuncuoğlu Şerefeddin Vocational School of Health Services, Amasya University, Amasya, Türkiye*

Keywords

Coumarin-PVA Interlayer

Surface States

Frequency and Voltage Dependency

Series Resistance

Abstract

Coumarin-PVA is deposited onto p-Si wafers using the spin coating technique. I examined the fundamental electrical variables of the Al/Coumarin–PVA/p-Si type Schottky barrier diodes (SBDs), by utilizing capacitance/voltage(*C-V*) and conductance/voltage (*G-V*) measurements at different frequencies varied from 10kHz to1MHz. I have thoroughly explored how the Coumarin–PVA interlayer, series resistance (*Rs*) and surface states (*Nss*) affect the electrical properties of SBDs. In order to remove R_s's influence on the observed C and G values, I corrected them. The observed high values of *C/G* measured at low frequencies result from the existence of interfacial states. There is evidence that while N_A decreases exponentially with increasing frequency, Φ_B increases exponentially. A particular distribution of N_{ss} density, polarization processes, and the existence of an interfacial layer can all contribute to explaining these characteristic features of them. According to experimental findings, I conclude that the interfacial polymer Coumarin–PVA layer as well as the N_{ss} and R_s also have a significant impact on the *C/G-V* quantities of SBDs.

Cite

Demirezen, S. (2023). The Study on the Wide Frequency Range of Electrical Variables in Al/Coumarin–PVA/p-Si Diodes at Room Temperature. *GU J Sci, Part A*, *10*(1), 53-61.

Author ID (ORCID Number)

S. Demirezen, 0000-0001-7462-0251

Article Process

Submission Date 11.11.2022
Revision Date 21.11.2022
Accepted Date 30.11.2022
Published Date 13.03.2023

1. INTRODUCTION

The search for high-performance electronic and optoelectronic devices has been evolving at an incredible pace thanks to new materials, architectures, manufacturing tools and processes. Advances in electronic systems aim at high density, high speed as well as reduced power dissipation. Due to their basis in electrical systems and ongoing importance in technology, much research has focus on semiconductors. Schottky barrier diodes (SBDs),known as metal/semiconductor (MS) contacts, offer several outstanding characteristics including very quick reaction time and low forward bias. The device becomes a metal/(metal-doped polymer)/semiconductor (MPS) SBD when there is a thin interfacial polymer film placed at the metal/semiconductor(M/S) interface. This interface layer can cause a biased interface state charge due to an extra electric field and affect the electrical properties of the diode (Sze, 1981; Sharma & Tripathi, 2013; Demirezen et al., 2022). Due to their use in the high-speed electrical, optoelectronic, and microelectronic industries, these diodes have surpassed metal/semiconductor (MS) type SBDs in importance. As a result, these gadgets' functionality is crucial. Therefore, current studies in this field have focused on device performance improvement with the use of interfacial layer/layers and complex preparation methods (Sharma & Tripathi, 2013).

As an interfacial polymer layer made of polyaniline, Poly (3-Substituted thiophene), polyvinyl-pyrrolidone, polyethylene-oxide, and polyvinyl alcohol (PVA) have attracted great interest from chemists, physicists and electrical engineers. Among these polymers, polyvinyl alcohol (PVA) has received a lot of interest due to its unique electrical and optoelectronic applications such as low cost, more charge-storage capacity, low molecular weight, nontoxicity, good film formation capacity, flexibility and ease of production process in

*Corresponding.Author, e-mail: selcukdemirezen@gmail.com

comparison with the other materials. Thus, it is widely exercised in fibber technology, paper, weaving, thin film plating and contact lens (Ashery et al., 2021).

Coumarin and its derivatives have become the focus of chemistry, physics, biology and medical research interest. This is because they exhibit numerous appealing features such as fluorescence in the electromagnetic spectrum's visible zone, high quantum yields and high solubility (Wang et al., 2005; Liu et al., 2012). Coumarin and their derivatives are also commonly utilized in sensors (Wang et al., 2005), dye lasers, organic light-emitting diodes (LEDs) (Liu et al., 2012), fluorescent markers, solar energy collectors, dye-sensitized solar cells (DSCs), and nonlinear optical applications (Ghouili et al., 2014).

In our earlier study (Demirezen & Altındal Yerişkin, 2020), we formed Al/p–Si (MS) structures with different Coumarin-PVA interlayer ratios (5, 10 and 20%) and compared their photovoltaic and electrical properties. We concluded that the %5 coumarin–PVA interlayer performed well in terms of higher RR and shunt resistance (R_{sh}) values as well as lower N_{ss} and R_s. In this sense, the main premise of this current study is to seek for more information on the capacitance/conductance-voltage characteristics for Al/(%5wt coumarin–PVA)/p-Si structures across in a wide range of frequency (10kHz-1MHz) and voltage (±5V by 0.05V steps).

2. MATERIAL AND METHOD

In this research, I constructed Al/(Coumarin–PVA)/p-Si structure onto the p-Si (Boron-doped) wafer. To achieve this, firstly, Al back contact was coated backside of the wafer in a vacuum environment (10^{-6} Torr) after that was annealed at 500°C to get lower-resistivity or better ohmic contact. Secondly, stirred (%5wt coumarin–PVA) solution was covered for 30 seconds at 2000 rpm and 80 ºC by using the Fytronix spin-coater system. After all, high-purity Al rectifier contacts with 0.785 mm^2 area were formed onto the interfacial layer. More information on the manufacturing procedures of these structures can be available in our former study (Demirezen & Altındal Yerişkin, 2020).

3. RESULTS AND DISCUSSION

In this study, I examined how the Coumarin–PVA interlayer, series resistance (*Rs*) and surface states (*Nss*) affect the electrical properties of SBDs. Based on the findings, Figure 1 displays The *C-V* and *G-V* curves of the Al/(Coumarin–PVA)/p-Si SBD at ambient temperature. As evident in these figs, both the frequency and voltage are more effective on the C/G variables. While the *C* and *G* exhibit significant dispersion in both the accumulation and depletion zones, they exhibit virtually complete frequency independent in the inversion region. In addition, *C-V* curves clearly show two peaks (weak and strong) that are located in the inversion and accumulation regions, respectively. The first peak (weak peak) can be attributed to a particular dispersion of N_{ss} at the interface and dipole or surface polarization, particularly at lower frequencies. The second peak (strong peak) can be ascribed to the R_s and interface layer. Additionally, in the meantime, peak positions show differences because of the rearrangement of the N_{ss} with direct current(dc) electric field, shifting towards the accumulation zone. On the other hand, the magnitude of these peaks decreases with increasing frequency. This results from the N_{ss} which cannot comply with the applied alternating field and does not supply an extra capacitance (C_{ex}) and conductance ($G_{ex.}/\omega$) (Card & Rhoderick, 1971; Nicollian & Brews, 1982).

In order to see the frequency dependency of capacitance and conductance more clearly, *C* and *G* data versus frequency were plotted between -1V and 4V by 0.5V steps. Figures 2a and 2b show frequency-dependent *C* and G/ω plots. As shown in these graphs, the *C* and G/ω values diminish with increasing frequency because the surface states comply with the applied alternating field at lower frequencies, therefore supplying an excess capacitance.

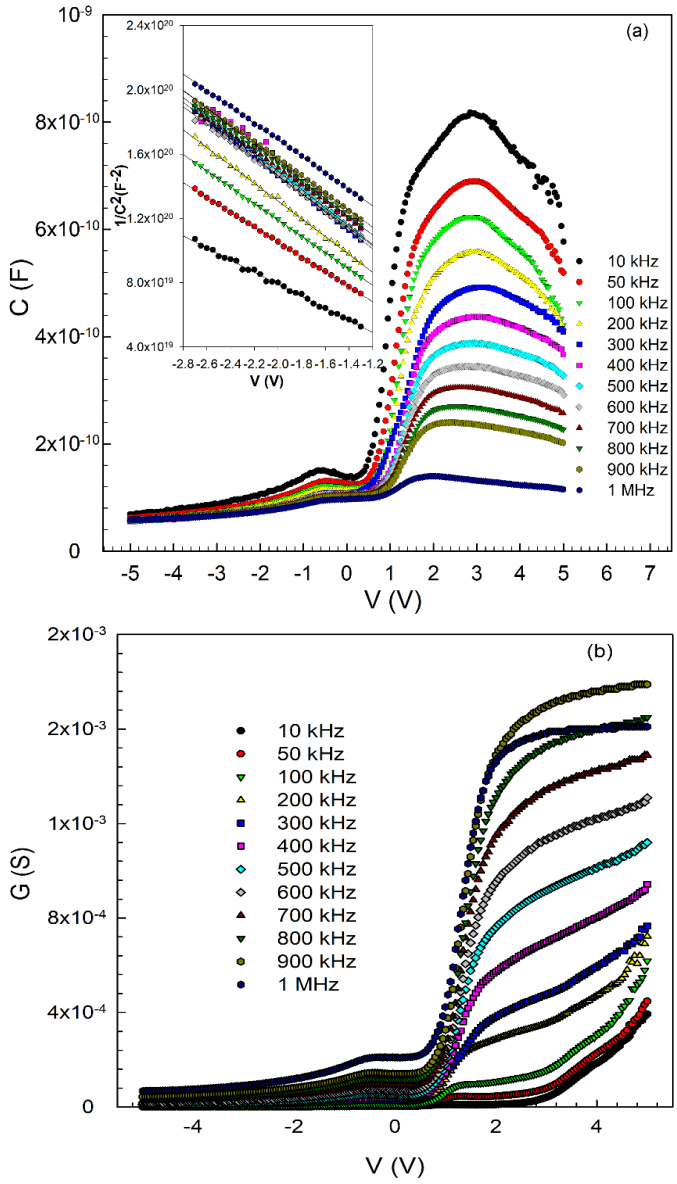

Figure 1. *The applied bias voltage dependent* ***a)*** *C-V,* ***b)*** *G-V curves of the Al/Coumarin–PVA/p-Si SBD*

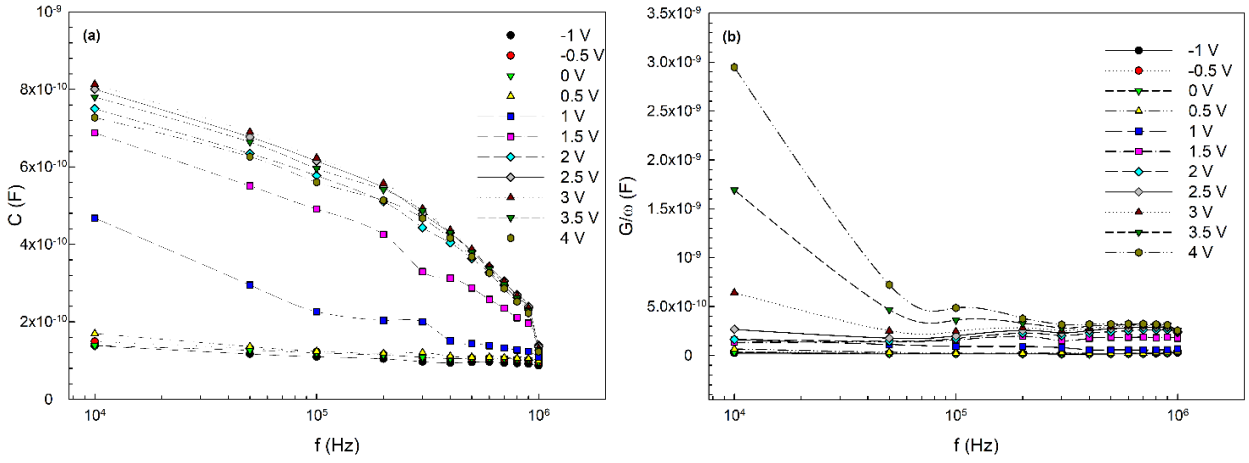

Figure 2. a) *Capacitance-frequency and*
b) *Conductance-frequency plots of the Al/(Coumarin–PVA)/p-Si SBD*

As mentioned above, R_s can have a significant impact on the C and G measurements, particularly at high frequencies in the accumulation zone/regime. The most popular technique for avoiding this inaccuracy is to measure R_s and then use it to alter the values of measured *Cm* and Gm/ω in a strong accumulation zone. As developed by Nicollian and Brews (1982), the subsequent equation may also be used to extract the voltage-dependent resistance (R_i) of the MIS type:

$$R_i = \frac{G_m}{G_m^2 + \left(\omega C_m\right)^2} \tag{1}$$

Using this approach, the R_s matches to the real R_i, particularly in the accumulation zone and above 500 kHz frequency. The angular frequency is denoted in this equation ω (=2π*f*), and the *C* and *G* are represented by C_m and G_m/ω in the strong accumulation zone. Thus, applied bias voltage and frequency-dependent R_s values were calculated and depicted in Figures 3a and 3b, respectively.

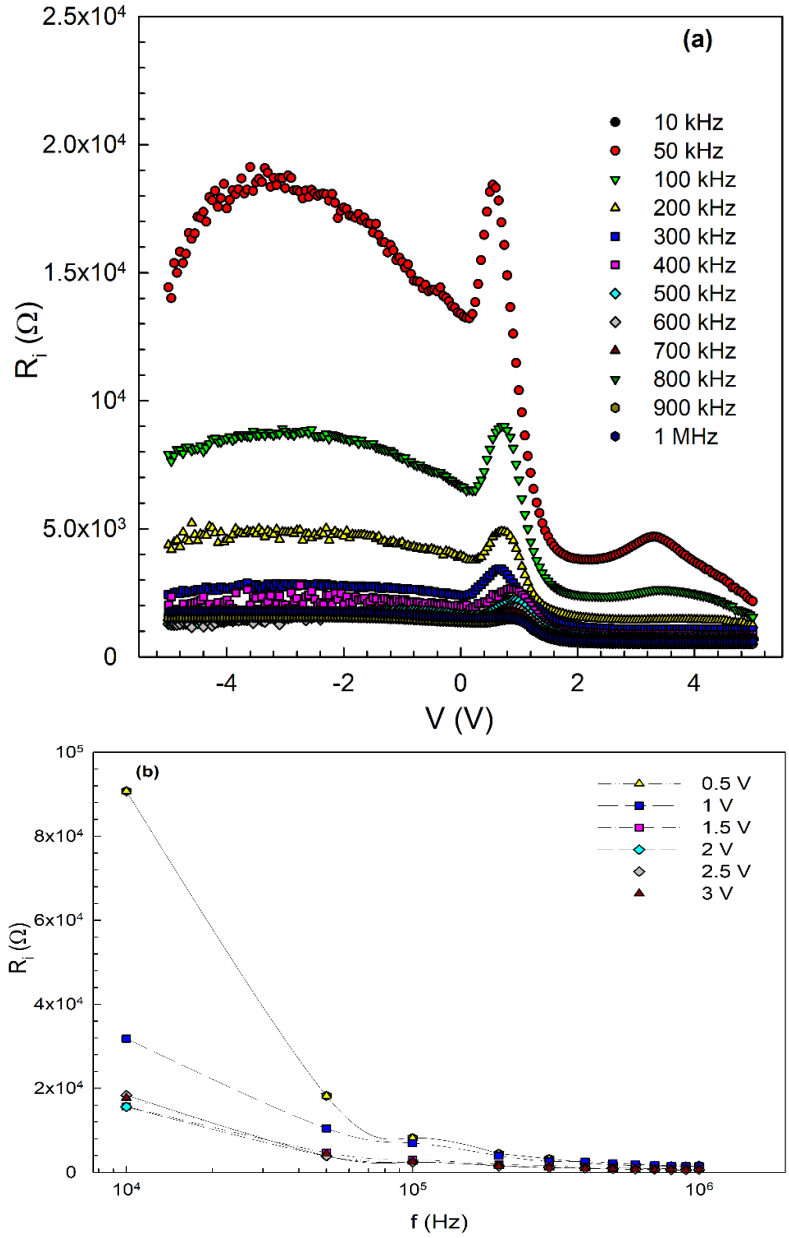

Figure 3. *The experimental R_i-V curves* ***a)*** *applied bias voltage dependency,* ***b)*** *frequency dependency of the Al/(Coumarin–PVA)/p-Si SBD*

Figures 3a and 3b shows that both in the depletion and accumulation zones the R_s value decreases as the frequency increases. Further, as shown in Figure 3a, the R_i curves exhibit a distinct peak and its magnitude decreases with increasing frequency and peaks tend to move in the direction of the accumulation zone as a result of the reorganization and reconstructing of N_{ss} under an electric field. This is due to the frequency and relaxation time (τ) of surface states, electronic charges in these states/traps can comply with an external ac signal at weak frequencies. Therefore, interfacial dipoles have less time at high frequencies to get into a position parallel to the alternative electrical field (Sze, 1981). For each applied bias voltage, R_i values decrease as frequency increases, as shown in Figure 3a and reach a constant value at the high forward bias (powerful accumulation zone). Therefore, the real R_s values correspond to accumulation at 5 V and are given at Table 1. Equation 1 can be used to correct C_m and G_m values by considered the value of R_s in order to avoid Rs effects on the real values of them.

$$C_c = \frac{\left[G_m^2 + (\omega C_m)^2\right] C_m}{a^2 + (\omega C_m)^2} \tag{2a}$$

$$G_c = \frac{G_m^2 + (\omega C_m)^2 a}{a^2 + (\omega C_m)^2} \tag{2b}$$

where a's value is supplied in the following form (Nicollian & Brews, 1982).

$$a = C_m - \left[G_m^2 + (\omega C_m)^2\right] R_s \tag{2c}$$

There is evidence to suggest that the R_s is the most critical factor responsible for the non-ideal electrical properties of SBDs. With a view to get the correct diode capacitance (C_c) and conductance (G_c), the C_m and G_m values were obtained by considering R_s influence by using Equation 2 and given in Figures 4a and 4b for 1 MHz. As can be seen in Figure 4a, the corrected C value increase as the bias voltage increases especially at the accumulation zone for the elimination Rs effect. I conclude that R_s can influence C and G measurements in depletion and accumulation zones at high frequencies, and therefore, this must be considered while calculating the electric and dielectric characteristics.

The straight-line part of C^{-2}-V graphs (inset Figure 1a) with different frequencies give important electrical characteristics of SBD, such as Φ_B, diffusion potential (V_D), Fermi energy level (E_F), depletion layer width (W_D) and concentration of acceptor atom (N_A). The C^{-2}-V curves display well linear behavior and are extrapolated to the voltage axis to determine the V_D values (Sze, 1981). One way to express the SBD depletion layer width is as follows:

$$W_D = \sqrt{\frac{2\varepsilon_s V_D}{qN_A}} \tag{3}$$

The N_A values may be computable via C^{-2}-V plot's slope for all frequencies. Hence, the E_F and N_A quantities were determined at various frequencies via following relations (Sze, 1981):

$$V_0 = V_D - \frac{kT}{q} \tag{4}$$

and E_F may be given as:

$$E_F = \frac{kT}{q}\ln(\frac{N_V}{N_A}) \tag{5}$$

with

$$N_V = 4.82x10^{15}T^{3/2}\left[\frac{m_h^*}{m_0}\right]^{3/2} \tag{6}$$

where N_V is the effective density state in the Si valance band, $m_h^* = 0.16m_0$ is the effective mass for holes (Sze, 1981), and m_0 ($9.1x10^{-31}$ kg) is the electron's rest mass.

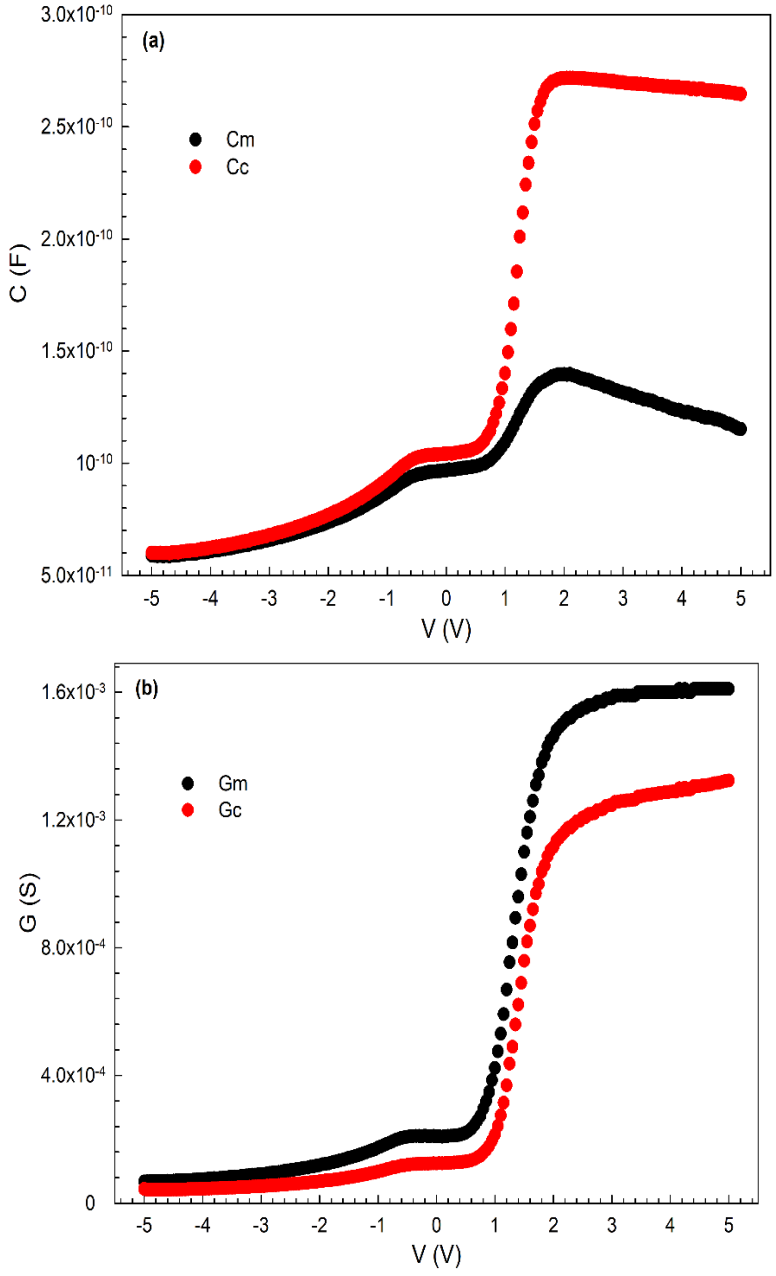

Figure 4. *Voltage dependent* ***a)*** *C_c and* ***b)*** *G_c/ω curves (without R_s) of the Al/(Coumarin–PVA)/p-Si SBD*

$$N_A = \frac{2}{q\varepsilon_s A^2 \tan(\theta)} \tag{7}$$

Here, ε_s is the permittivity of the Si. As a result, the following relation may be utilized to determine the Φ_B values for each frequency:

$$\Phi_B(C-V) = V_D + E_F \tag{8}$$

Table 1 lists the obtained V_D, N_A, E_F, W_D and $\Phi_B(C\text{-}V)$ parameters for each frequency. This kind of N_A and $\Phi_B(C\text{-}V)$ behavior is predicted and is ascribed to the specific density dispersion of N_{ss} and the interfacial layer (Çokduygulular et al., 2020; Cetinkaya et al., 2022).

Table 1. *The frequency dependent some electric quantities of the Al/(Coumarin–PVA)/p-Si SBD*

f (kHz)	**N_A (cm^{-3})**	**V_D (eV)**	**E_F (eV)**	**W_D (cm)**	**Φ_B (eV)**	**Rs (Ω)**	**Nss ($eV^{-1}cm^{-2}$)**
10	5.13×10^{15}	0.21	0.15	2.28×10^{-5}	0.32	2541.78	7.73×10^{13}
50	4.25×10^{15}	0.31	0.15	3.09×10^{-5}	0.41	2163.57	1.76×10^{13}
100	4.12×10^{15}	0.45	0.15	3.77×10^{-5}	0.54	1545.69	1.22×10^{13}
200	4.02×10^{15}	0.58	0.16	4.33×10^{-5}	0.67	1223.62	7.11×10^{12}
300	3.99×10^{15}	0.69	0.16	4.72×10^{-5}	0.78	1041.29	5.02×10^{12}
400	3.96×10^{15}	0.74	0.16	4.90×10^{-5}	0.82	856.48	4.64×10^{12}
500	3.95×10^{15}	0.82	0.16	5.17×10^{-5}	0.91	737.99	4.41×10^{12}
600	3.93×10^{15}	0.84	0.16	5.26×10^{-5}	0.93	649.72	4.30×10^{12}
700	3.69×10^{15}	0.87	0.16	5.51×10^{-5}	0.95	586.98	4.19×10^{12}
800	3.68×10^{15}	0.90	0.16	5.64×10^{-5}	0.99	541.46	4.06×10^{12}
900	3.57×10^{15}	0.97	0.16	5.94×10^{-5}	1.05	507.04	3.92×10^{12}
1000	3.56×10^{15}	1.02	0.16	6.08×10^{-5}	1.10	591.28	3.17×10^{12}

In this work, the Hill-Coleman approach was also employed to obtain the Nss for each frequency and are also tabulate in Table 1 (Hill & Coleman, 1980):

$$N_{SS} = \frac{2}{qA}\frac{(G/\omega)_m}{\left\{\left[(G/\omega)_m/C_i\right]^2 + (1-C_m/C_i)^2\right\}} \tag{9}$$

where the contact area represented by A, angular frequency represented by $\omega=2\pi f$, capacitance and conductance represented by C_m and G_m/ω that in line with the peak values, respectively. Interfacial layer capacitance (C_i) calculated from the strong accumulation zone as (Hill & Coleman, 1980):

$$C_i = C_m\left[1+\frac{G_m^2}{(\omega C_m)^2}\right] = \frac{\varepsilon_i \varepsilon_o A}{d} \quad (10)$$

Table 1 shows the R_s (at 5 V) and N_{ss} (V) which are corresponding to the peak value of *C-V* plots as functions of frequency by using Equations 1 and 9, respectively. As indicated in the table, the values of N_{ss} and R_s decrease as frequency increases. This R_s behavior is caused by the interfacial layer and a special dispersion of interface states densities among organic and inorganic semiconductor interfaces (Sze, 1981). Based on these findings, I conclude that both the R_s and N_{ss} values represent greater efficacy on *C-V* and *G-V* measurements and have the potential to affect calculations significantly.

4. CONCLUSION

The *C-G/ω-V* measurements of the Al/(Coumarin-PVA)/p-Si SBD were implemented at ambient temperature in the frequency 1 kHz- 1 MHz range. All of these measurements were performed between (-5V) and (+5V) by 0.05V increment. The effect of Coumarin–PVA interlayer, R_s and N_{ss} on electrical characteristics of the SBD have been investigated in detail. R_s-*V* plots which acquired using the *C* and *G* values displayed a peak behavior at each frequency. These peak magnitudes decrease as the frequency increase in the depletion zone. The observed C and G values were corrected as C_c and G_c by considering Rs for 1MHz. Moreover, the observed lower C and G values at lower frequencies were ascribed to the existence of N_{ss} and polarization processes. While the Φ_B(*C-V*) values exponentially increase with increasing frequency the N_A value decreases. This predicted propensity of N_A and Φ_B(*C-V*) is explained by a special density distribution of N_{ss} between p-Si and organic interfacial layer, dipole and surface polarization. The acquired experimental results provide evidence to suggest that the Coumarin–PVA layer has a significant effect on the *C-V* and *G-V* measurements of SBDs, as well as R_s and N_{ss}.

ACKNOWLEDGEMENT

This work has received funding from Amasya University Scientific Research Projects with the reference number FMB-BAP 17-0292. Some part of this study is presented at **MSNG-2022**.

REFERENCES

Ashery, A., Gad, S. A., & Turky, G. M. (2021). Analysis of Electrical and Capacitance–Voltage of PVA/nSi. *Journal of Electronic Materials*, *50*(6), 3498-3516. doi:10.1007/s11664-021-08867-y

Card, H. C., & Rhoderick, E. H. (1971). Studies of tunnel MOS diodes I. Interface effects in silicon Schottky diodes. *Journal of Physics D: Applied Physics*, *4*(10), 1589-1601. doi:10.1088/0022-3727/4/10/319

Cetinkaya, H. G., Cicek, O., Altindal, S., Badali, Y., & Demirezen, S. (2022). Vertical CdTe:PVP/ p -Si-Based Temperature Sensor by Using Aluminum Anode Schottky Contact. *IEEE Sensors Journal*, *22*(23), 22391-22397. doi:10.1109/JSEN.2022.3212867

Çokduygulular, E., Çetinkaya, Ç., Yalçın, Y., & Kınacı, B. (2020). A comprehensive study on Cu-doped ZnO (CZO) interlayered MOS structure. *Journal of Materials Science: Materials in Electronics*, *31*(16), 13646-13656. doi:10.1007/s10854-020-03922-6

Demirezen, S., Çetinkaya, H. G., & Altındal, Ş. (2022). Doping rate, Interface states and Polarization Effects on Dielectric Properties, Electric Modulus, and AC Conductivity in PCBM/NiO:ZnO/p-Si Structures in Wide Frequency Range. *Silicon*, *14*(14), 8517-8527. doi:10.1007/s12633-021-01640-0

Demirezen, S., & Altındal Yerişkin, S. (2020). A detailed comparative study on electrical and photovoltaic characteristics of Al/p-Si photodiodes with coumarin-doped PVA interfacial layer: the effect of doping concentration. *Polymer Bulletin*, *77*(1), 49-71. doi:10.1007/s00289-019-02704-3

Ghouili, A., Dusek, M., Petricek, V., Ayed, T. B., & Hassen, R. B. (2014). Synthesis, crystal structure and spectral characteristics of highly fluorescent chalcone-based coumarin in solution and in polymer matrix. *Journal of Physics and Chemistry of Solids*, *75*(2), 188-193. doi:10.1016/j.jpcs.2013.09.011

Hill, W. A., & Coleman, C. C. (1980). A single-frequency approximation for interface-state density determination. *Solid-State Electronics*, *23*(9), 987-993. doi:10.1016/0038-1101(80)90064-7

Liu, X., Cole, J. M., Waddell, P. G., Lin, T.-C., Radia, J., & Zeidler, A. (2012). Molecular Origins of Optoelectronic Properties in Coumarin Dyes: Toward Designer Solar Cell and Laser Applications. *The Journal of Physical Chemistry A*, *116*(1), 727-737. doi:10.1021/jp209925y

Nicollian, E. H., & Brews, J. R. (1982). *Metal oxide semiconductor (MOS) physics and technology*. Wiley.

Sharma, M., & Tripathi, S. K. (2013). Analysis of interface states and series resistance for Al/PVA: N-CdS nanocomposite metal-semiconductor and metal-insulator-semiconductor diode structures. *Applied Physics A: Materials Science & Processing*, *113*(2), 491-499. doi:10.1007/s00339-013-7552-3

Sze, S. M. (1981). *Physics of Semiconductor Devices* (2nd Ed.). Wiley.

Wang, Z.-S., Hara, K., Dan-oh, Y., Kasada, C., Shinpo, A., Suga, S., Arakawa, H., & Sugihara, H. (2005). Photophysical and (Photo)electrochemical Properties of a Coumarin Dye. *The Journal of Physical Chemistry B*, *109*(9), 3907-3914. doi:10.1021/jp044851v